PRECIPITATION SIMULATION AND X-RAY ABSORPTION SPECTROSCOPY FOR HOT ROLLED V-HSLA STEEL

Piyada Suwanpinij[1)], Hans Henning Dickert[2),3)] Prasonk Sricharoenchai[4)]*
[1)] The Sirindhorn International Thai-German Graduate School of Engineering (TGGS), King Mongkut's University of Technology North Bangkok (KMUTNB), Bangkok, Thailand
[2)] Department of Ferrous Metallurgy, RWTH Aachen University, Aachen, Germany
[3)] Georgsmarienhütte GmbH, Georgsmarienhütte, Germany
[4)] Department of Metallurgical Engineering, Chulalongkorn University, Bangkok, Thailand

Received: 23.10.2016
Accepted: 16.11.2016

[*]Corresponding author: *e-mail:* piyada.s@tggs.kmutnb.org, *Tel: +66 2 555 2000, ext 2918, TGGS, KMUTNB, 1518 Pracharat Sai 1, Bangkok, 10800, Thailand*

Abstract
Aiming to the process optimisation while reducing or avoiding experimental work, the work has been carried out by a physically-based thermokinetic model proven by synchrotron X-ray absorption spectroscopy. The mole fraction and size distribution of different precipitate species as well as the consumption of the dissolved elements are of the main interest. The model considers the involved parameters in the hot rolling process, i.e., austenite grain size, disloca-tion density as a function of deformation, and thermal history during the process. Both grain boundary and dislocation are nucleation sites. The diffuse interface effect on the interfacial energy as well as a volumetric misfit of AlN at dislocations is also taken into account. The latter is because of its significant difference in the lattice parameter from the matrix. The X-Ray absorption spectroscopy (XAS) taken advantage from the synchrotron technology has been employed for the quantification of the precipitation of vanadium as well as its fraction in the solid solution. With very good agreement, V(C,N) precipitates significantly due to high dislocation and is not overridden by the competing AlN.

Keywords: precipitation simulation, high strength low alloyed steel, hot rolling, vanadium, X-ray absorption spectroscopy

1 Introduction

High strength low alloyed (HSLA) steels are well-known to inherit their high strength from precipitation hardening and grain refinement mechanisms. Both are the results of the precipitation of their microalloying elements [1-4], from which vanadium and titanium are selected for the steel concept. Optimisation of the precipitation along a processing route is therefore important to enhance the strength and toughness by considering cost minimisation. This work combines the thermokinetic simulation with a new alternative experimental inves-tigation of precipitates in a vanadium-containing HSLA steel. This is to demonstrate the pre-cipitation analysis without too much laborious experimental work.

Although a large number of precipitation models in metal are available, most of them still need phenomenological fitting parameters that require several experiments for each. The selected thermokinetic models contained in the software package MatCalc are claimed to be independent from these fitting parameters and therefore are selected for the simulation. This approach has been studied in several different microalloying concepts in ferrous and non-ferrous systems [5-12].

DOI 10.12776/ams.v22i4.817 p-ISSN 1335-1532
e-ISSN 1338-1156

Different precipitation phenomena during metal processing, e.g., primary precipitation during solidification [10], dissolution during austenitisation [8], solute drag and recrystallisation [11], precipitation during ageing and tempering [7] have been comprehensively studied and validated for the models. The effect of deformation which multiplies the density of dislocation is also of interest [6, 13-14] as dislocation is a major nucleation site and accelerates the precipitation.
The precipitation modelling results are usually validated with the experimental results by means of different conventional characterisation methods, i.e., TEM, EDS, DSC as well as different microscopic techniques corresponding to the size of the concerning precipitates [7,9,11,13-14]. If the concentration of different atoms is required, an advanced method like Atom Probe Tomography (APT) [13,14] is carried out. Alternatively, the investigation by X-Ray Absorption Spectroscopy (XAS) from synchrotron source can be used to confirm the simulation results in this work as shown earlier [5]. It is relatively new to quantify the fraction of precipitates in metals.

2 Experimental Process Simulation

A steel microalloyed with vanadium and titanium was cast in a vacuum induction melting furnace, followed by repeated hot forging. The chemical composition of the steel is listed in **Table 1**.

Table 1 The chemical composition of the simulated steel, in mass%.

Material Name	C	Si	Mn	P	S	Cr	Mo	Al	Ti	V	N
V- HSLA	0.070	0.05	0.98	0.0055	0.0033	0.50	0.010	0.0334	0.011	0.10	0.0240

The process simulation of the hot rolling was carried out in a deformation dilatometer Bähr DIL 805 A/D using homogenised cylindrical samples with a diameter of 5 mm and a length of 10 mm. A few deformation steps were applied at higher temperature with a long interpass time to ensure enough recrystallisation prior to a deformation below the non-recrystallisation temperature, T_{nr}, with a logarithm strain of 0.3 according to the thermomechanical cycles in **Fig. 1** and the listed parameters in **Table 2**. Different cooling rates were varied after the isothermal period simulating the Run Out Table (ROT) for their influences of the vanadium precipitation.

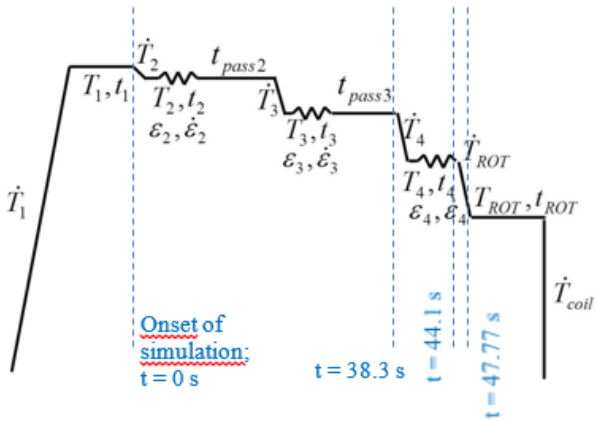

$\dot{T}_1, T_1, t_1$	200 °C/minute, 1250 °C, 15 minute
$\dot{T}_2, T_2, t_2$	5 °C/s, 1200 °C, 3 s
$\varepsilon_2, \dot{\varepsilon}_2, t_{pass2}$	0.2, 12 s^{-1}, 10 s
$\dot{T}_3, T_3, t_3$	60 °C/s, 1150 °C, 3 s
$\varepsilon_3, \dot{\varepsilon}_3, t_{pass3}$	0.4, 12 s^{-1}, 10 s
$\dot{T}_4, T_4, t_4$ (Retained strain)	60 °C/s, 900 °C, 3 s
$\varepsilon_4, \dot{\varepsilon}_4, t_{pass4}$	0.3, 12 s^{-1}, 0 s
$\dot{T}_{ROT}, T_{ROT}, t_{ROT}$ (Run Out Table)	60 °C/s, 680 °C, 6 s
$\dot{T}_{coil}$ (Coiling)	0.1/ 5/ 60 °C/s

Fig. 1 The thermomechanical cycles adopted in the simulation to simulate the precipitation, shown with **Table 2** the thermomechanical process parameters

DOI 10.12776/ams.v22i4.817 p-ISSN 1335-1532
e-ISSN 1338-1156

3 Thermokinetic Simulation

3.1 Classical nucleation model

The classical nucleation theory (CNT) [16-17] is adopted for the nucleation kinetics and extended for multi-component systems [17-19] as follows:

$$J = N_0 Z \beta^* exp\left(\frac{-G^*}{k_B T}\right) exp\left(\frac{-\tau}{t}\right). \quad (1.)$$

The symbol J stands for the nucleation rate, or how many nuclei are created per unit volume and time. N_0 represents the total density of potential nucleation sites. T is the temperature, k_B the Boltzmann constant and t is the time. The Zeldovich factor Z takes into account that the nucleus is destabilised by thermal excitation as compared with the inactivated state. The variable τ is incubation time, while the critical Gibbs free energy for nucleus formation G^* is

$$G^* = \frac{16\pi}{3} \frac{\gamma^3}{(\Delta G_{vol} - \Delta G_S)^2}, \quad (2.)$$

which depends on with the effective interfacial energy γ, the volume free energy change ΔG_{vol} and the misfit strain energy ΔG_s.

The interfacial energy, γ, is calculated from the generalised n-nearest-neighbour broken-bond model developed by Sonderegger and Kozeschnik [20]. It is a function of composition and temperature and can be calculated from

$$\gamma = \frac{n_S Z_{S,eff}}{N_A Z_{L,eff}} \cdot \Delta H_{sol}. \quad (3.)$$

Hence, the interfacial energy determined by the product of the enthalpy of solution ΔH_{sol} and the factor $\frac{n_S Z_{S,eff}}{N_A Z_{L,eff}}$. The enthalpy is thermodynamic variable which can be calculated from CALPHAD database [21]. On the other hand, the term n_S is the number of atoms per unit area of the interface. The term $z_{S,eff}$ is the effective number of broken bonds across the interface counted per interface atom, while $z_{L,eff}$ is the effective coordination number [20] and N_A is Avogadro's number.

3.2 Mean field model for growth

The growth of the nucleated precipitate is evaluated based on a mean-field approach derived by Svoboda [22] from which the radius and composition of the precipitate evolve. This approach describes the total Gibbs free energy of a thermodynamic system G with n components and m precipitates as

$$G = \sum_i^n N_{0i}\mu_{0i} + \sum_{k=1}^m \frac{4\pi\rho_k^3}{3}(\lambda_k + \sum_{i=1}^n c_{ki}\mu_{ki}) + \sum_{k=1}^m 4\pi\rho_k^2\gamma_k. \quad (4.)$$

The term μ_{0i} is the chemical potential of component i in the matrix and μ_{ki} is the chemical potential of component i in the precipitate k. The chemical potentials are functions of the concentrations c_{ki}. The term γ means the interface energy density and λ_k accounts for the contribution of the elastic energy and plastic work due to the volume change of each evolving precipitate.

The change into a more stable state can take place and the excess free energy will results in: interface movement, diffusion inside the precipitate and diffusion inside the matrix [22]. The software package MatCalc employs the numerical time integration of the evolution equations based on the classical numerical Kampmann–Wagner approach [23].

DOI 10.12776/ams.v22i4.817 p-ISSN 1335-1532
e-ISSN 1338-1156

3.3 Dislocation model

The increase in the dislocation density under deformation can be described by the so-called one parameter model [24] or

$$\frac{d\rho}{dt} = \left(\frac{M\dot{\varepsilon}}{bL}\right), \tag{5.}$$

where M is the Taylor factor, which is 3.06 for FCC crystals [25], $\dot{\varepsilon}$ is the strain rate and b is Buger's vector. The travelling distance L can be calculated from the dislocation density and a material constant ranging from 50 to 100. The emerging dislocation density is annihilated by the opposing dislocations with antiparallel Burger's vectors as well as by thermally activated dislocation climb [26].

3.4 Simulation set-up

The precipitation simulation was performed in MatCalc version 5.60 with the thermodynamic database and diffusion database mc_fe [21, 27]. Titanium was not put into the system as it forms TiN, which is well-known to form during the solidification and not dissolved during the reheating. The nitrogen content put into the system is therefore reduced from the nominal composition into 0.015 mass%. Labelled in the thermomechanical cycle in **Fig.1**, the simulation starts from cooling down from 1250 °C. Only sharp transformation temperature can be set up in the calculation. Hence, the simulated temperature of Run Out Table (ROT), T_{ROT}, of 680 °C was chosen for changing the precipitation domain from austenite into ferrite, as ferrite was only little to observed before reaching this isothermal period.

The precipitation of AlN and V(C,N) is both at grain boundaries and dislocations in both austenite and ferrite parent phases, while that of cementite is at dislocations only. The grain sizes of 100 μm and 10 μm were selected for austenite and ferrite, respectively. The equilibrium dislocation density in austenite was assigned as 10^{11} m^{-2} while that in ferrite as 10^{12} m^{-2}. The volumetric misfit of only AlN at dislocations was considered, which is 0.27 due to different lattice size. As the critical temperature is recommended to take into account for the calculation of interfacial energy due to the diffuse interface, a critical temperature of 1727 °C was selected for V(C,N) as an estimation from those reported for VC and VN in both austenite and ferrite [28]. It indicates the highest temperature at which two phases are present in the system, regardless of the composition. The number of size class was selected as 25 for all precipitating species as it is adequate for good simulation quality with reasonable calculation time.

4 Characterisation of the Precipitate

4.1 Principle of XAS

The XAS spectrum records a photoelectric absorption in the investigated atoms. While scanning the synchrotron X-ray from lower to higher energy, which is just above binding energy between core-level electron and nucleus in an atom, the X-ray photon energy will be absorbed and then knock the core electron out as a photoelectron. This absorption will be seen as a sharp rise at characteristic specific energy, a so-called absorption edge, in the spectrum (**Fig.2**). The emitted photoelectron causes a core-hole in the electron shell that results another electron from the outer shells to replace the lost electron, emitting out fluorescent X-ray.

The X-ray Absorption Near Edge Spectroscopy (XANES) in **Fig.2** is the region near the absorption edge. The shift in energy of the absorption edge indicates the type and oxidation state of the absorbing atoms [29-30]. More structural information can be obtained from the oscillation

DOI 10.12776/ams.v22i4.817 p-ISSN 1335-1532
e-ISSN 1338-1156

in the Extended X-ray Absorption Fine Structure (EXAFS) structure which is extended far behind the absorption edge and can be considered as a fingerprint of substance. This is due to the scattering phenomenon between the emitted photoelectron from the central atom and the surrounding atoms. In a mixture with more than one phase containing the absorbing atom, the EXAFS shows the summation of fingerprint spectra of those compounds in the mixture.

5 The XAS measurement

XAS measurements were carried out at beamline BL8 of the Siam Photon Laboratory (SPL) at Synchrotron Light Research Institute (SLRI), Nakhon Rachasima, Thailand [31]. The SPL ring operates with an electron energy of 1.2 GeV with a beam current of 150-80 mA. The experiment was setup to measure the vanadium precipitates in the samples with different cooling rates and polished until with 1 μm Al_2O_3 in suspension.

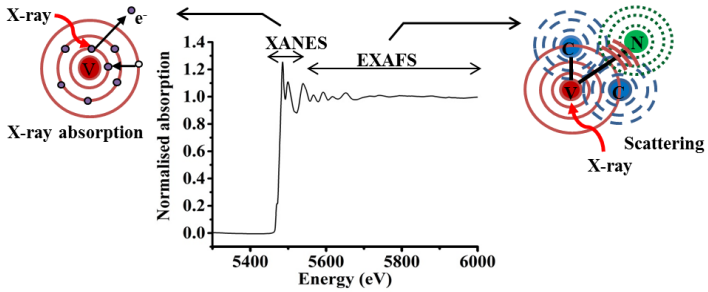

Fig. 2 Schematic representation of the XAS spectrum composing of XANES and EXAFS

A solution-annealed sample, employed as a standard for vanadium solute atoms in the solid solution, and the steel samples with three different cooling rates, i.e. 60, 5 and 0.1 °C/s, were selected to measure vanadium K-edge absorption spectra in a fluorescent mode. A beam with a cross section of 1 × 16 mm penetrating down to 100 μm results in an illuminated volume of 1.6 mm^3 [15] Standard powdered compounds of VC, VN and V(C,N) were prepared in a thin layer film and then measured in transmission mode as the standard spectra for the Linear Combination Fit (LCF). The solution-annealed sample can be used for the standard spectrum of vanadium in solid solution as proven earlier in [32].

6 Simulation Results

According to the dislocation model, the dislocation density gradually drops after long interpass time, during which the recovery takes place. However, at the end of the interpass time, the dislocation density is still of 1 order of magnitude higher than the equilibrium state. With the logarithm strain of 0.3 at 900 °C, the dislocation density reaches 3.62×10^{14} m^{-2}, which means the increases in the dislocation density with 2 orders of magnitude. Hence, there are a large number of nucleation sites at dislocation.

The mole fraction of the precipitates was calculated from all phases in the system, including the matrix. Although difficult to notice from the scale of the plotted diagrams, the precipitation of V(C,N) starts after 38.3 s along the assigned thermomechanical process or at 1063 °C in the austenitic state. The dominating precipitating group is the V(C,N) at dislocations and results in the consumption of V(C,N) at the grain boundaries. This is difference from what that found by

DOI 10.12776/ams.v22i4.817 p-ISSN 1335-1532
e-ISSN 1338-1156

Radis et al. [33], whose case shows that the predominant site of AlN is only grain boundaries and the precipitation of AlN at dislocations overrides that of V(C,N).

From 47.77 s, the start of the period on the ROT, the matrix turns to be completely ferritic. **Fig. 3**(d) and (e) are just below 4(a) and (b), respectively, at identical time scale to visualise the consumption of vanadium in the solid solution. The site fraction in the sublattices of the BCC iron under the cooling rate of 60 and 5 °C/s are plotted. The first sharp drop in the concentration of vanadium in the solid solution attributes to the isothermal temperature of 680 °C, which simulates the period on the ROT. This part attributes to 60% of the total dissolved content. Comparing to the thermomechanical cycle, the last sharp drop to the lowest concentration is just above 660 °C.

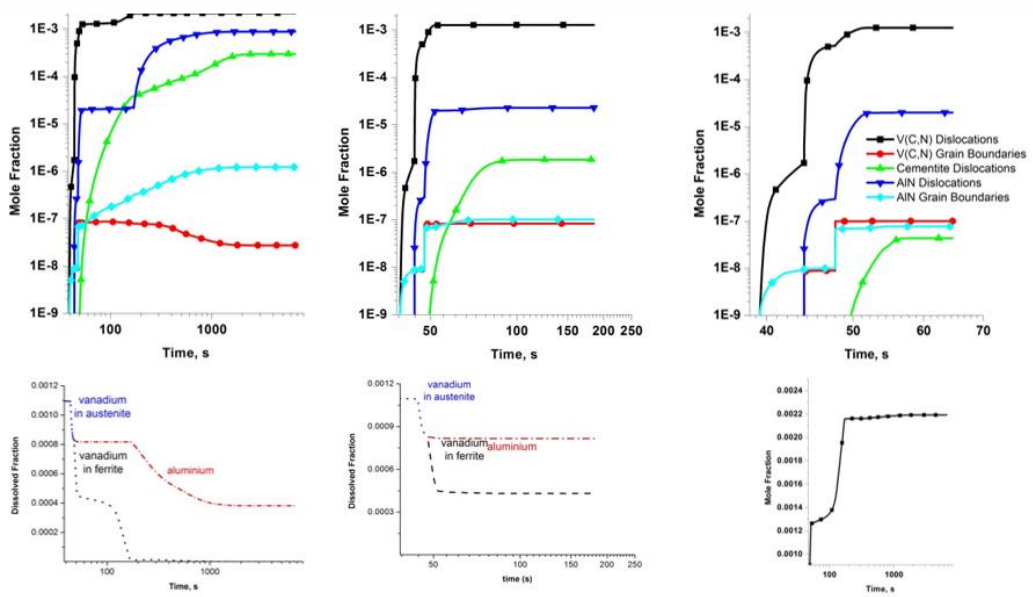

Fig. 3 The mole fraction of the precipitates, under different cooling rates a) 0.1 °C/s, b) 5 °C/s, c) 60 °C/s, plotted during cooling from 1150 °C to 900 °C. The site fraction of the dissolved vanadium and aluminium in ferrite for the corresponding cooling rates are plotted below in d) and e) to time scale to visualise the element consumption. f) The precipitation of V(C,N) at dislocation after the matrix is changed totally into ferrite.

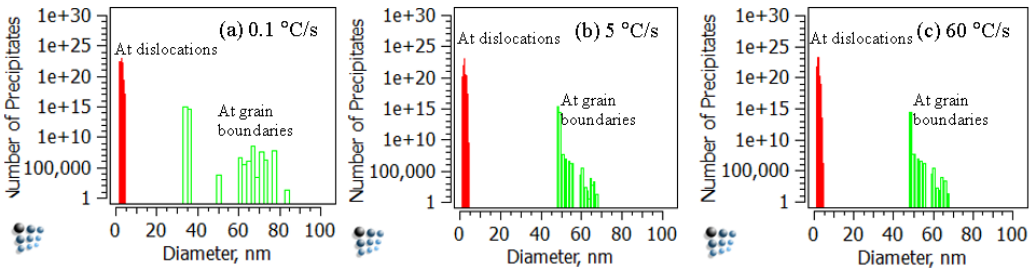

Fig. 4 The size distribution of V(C,N) at the end of the simulated hot rolling process under different cooling rates

DOI 10.12776/ams.v22i4.817
p-ISSN 1335-1532
e-ISSN 1338-1156

Fig. 3(f), plotted from 47.77 s, where ferrite starts, reveals that although V(C,N) starts to precipitate in austenite at higher temperature and give additional significant fraction after transforming into ferrite as a sharp rise due to higher diffusivity and dislocation density in ferrite. Very fine precipitates can be expected due to relatively low temperature in this period. **Fig. 4** reveals the size distribution of both groups of V(C,N): at dislocations and at grain boundaries. The group of V(C,N) at dislocations is below 5 nm in diameter and has a very narrow size range. Slow cooling rate enables a large size range of those at grain boundaries; 30 to 85 nm in diameter. The size range is much smaller, or 44 to 78 nm in diameter, under higher cooling rates.

7 Results of XAS Characterisation

The simulation results are compared with those from XAS measurement evaluated by LCF method in **Table 3**. The dissolved concentration of vanadium in the simulation is taken from the site fraction in the related sublattices of ferrite. Both follow the trend that slower cooling rates allow larger fraction of precipitate and leave smaller fraction of vanadium in the solid solution. Although VN and VC are not separate groups in the simulation, their fractions found by XAS are negligible. The high cooling rate of 60 °C/s from the simulation underestimates further precipitation at lower temperature. Contrarily, slowest cooling rate overestimates the results measured by the XAS.

Table 3 The mole fraction of the vanadium precipitates from the thermokinetic simulation and XAS

	Simulation		**XAS**					
$\dot{T}_{coil}$, **[°C.s^{-1}]**	**Dissolved V**	**V(C,N)**	**Dissolved V**	**V(C,N)**	**VN**	**VC**	**Sum**	**R-value**
60	0.418	0.582	0.638 ± 0.009	0.292 ± 0.013	0.000 ± 0.014	0.070 ± 0.022	1.000	0.0008725
5	0.395	0.605	0.306 ± 0.009	0.670 ± 0.013	0.004 ± 0.014	0.019 ± 0.021	1.000	0.0010298
0.1	0.0001	0.9999	0.042 ± 0.010	0.890 ± 0.015	0.072 ± 0.017	0.000 ± 0.014	1.004	0.0013560

8 Discussion

It can be clearly seen that the first 20 degree of temperature after cooling down from the ROT results in the main precipitation fraction of V(C,N). A cooling rate higher than 5 °C/s gives negligible difference. Therefore, the simulations with the cooling rates of 5 and 60 °C/s yield similar remaining concentration of vanadium in the solid solution but it overestimates the degree of precipitation under the cooling rate of 60 °C/s according to the results by XAS. According to the reported solubility data, vanadium precipitates as V(C,N), VN and VC at relatively low temperature compared with other microalloying elements [34-36] and hence is influenced in lower temperature region to a larger extent.

That the major part of the precipitation takes place in ferrite can be the advantage for very fine precipitates of V(C,N). Baker [35] confirms the presence of very fine precipitates that are not visible under transmission electron microscope, or can be easily lost during sample preparation. The nitrogen content taken into the simulation can be too low but it helps proving the possibility

DOI 10.12776/ams.v22i4.817 p-ISSN 1335-1532
e-ISSN 1338-1156

of taking advantage of vanadium precipitation without adding too much nitrogen, which is challenging in some production routes.

The discrepancies between the numerical simulation and experiment results can be from the difference in grain size, although to relatively small as the precipitation at grain boundaries is much less, and to a larger extent, the sharp transformation from austenite to ferrite. Moreover, albeit no phenomenological fitting parameter, it is important to know if there is other competing species such as AlN for VN as found by Radis et al. [33], whose case shows that the predominant site of AlN is only grain boundaries and the simulation of precipitation of AlN at dislocations would override that of VN, which brings significant discrepancy.

9 Conclusions

Both deformation and slow cooling rate promote the precipitation of vanadium significantly. The precipitation of V(C,N) at dislocations dominates the precipitation in the selected steel. Slow cooling rate allows further nucleation and enough time for the growth of the existing precipitates that the dissolved content of vanadium decreases.

The prediction by the selected thermokinetic models fit the finding of the precipitate content discovered by XAS fairly well. Therefore it shows to be a great powerful tool for the thermomechanical process optimisation to benefit from the precipitation while saving the number of experiments. Likewise, XAS proves itself to be a promising materials characterisation method for precipitation in metal too.

References

[1] R. H. J. Hannink, A. J. Hill: *Nanostructure Control of Materials*, 1st ed., Woodhead Publishing, Cambridge, 2006, p. 231

[2] J. Lu, O. Omotoso, J. B. Wiskel, D. G. Ivey, H. Henein: *Metallurgical and Materials Transactions A*, Vol. 43, 2012, No.9, pp. 3043-3061, doi: 10.1007/s11661-012-1135-3

[3] N. Kamikawa et al.: *Acta Materialia*, Vol. 83, 2015, No.1, p. 383-396, doi: 10.1016/j.actamat.2014.10.010

[4] P. A. Manohar, M. Ferry, T. Chandra: *ISIJ International*, Vol. 38, 1998, No.9, p. 913-924, doi: 10.2355/isijinternational.38.913

[5] G. Stechauner and E. Kozeschnik: *Acta Materialia*, Vol. 100, 2015, p. 135-146, doi: 10.1016/j.actamat.2015.08.042

[6] M. Lückl, S. Zamberger and E. Kozeschnik: *Steel Research International*, Vol. 87, 2016, No. 3, p. 271-275, doi: 10.1002/srin.201500041

[7] S. Zamberger, T. Wojcik, J. Klarner, G. Klösch, H. Schifferl, E. Kozeschnik: *Steel Research International*, Vol. 84, 2013, No.1, pp. 20-30. doi: 10.1002/srin.201200047

[8] P. Lang, M. Rath, E. Kozeschnik, P.E.J. Rivera-Diaz-del-Castillo: *Scripta Materialia*, Vol.101, 2015, pp. 60-63, doi: 10.1016/j.scriptamat.2015.01.019

[9] P. Lang, T. Wojcik, E. Povoden-Karadeniz, A. Falahati, E. Kozeschnik: *Journal of Alloys and Compounds*, Vol. 609, 2014, pp.129-136, doi: 10.1016/j.jallcom.2014.04.119

[10] S. Zamberger, M. Pudar, K. Spiradek-Hahn, M. Reischl, E. Kozeschnik: *International Journal of Materials Research*, Vol.103, 2012, No. 6, pp. 680-687, doi: 10.3139/146.110688

[11] A. Timoshenkov, P. Warczok, M. Albu, J. Klarner, E. Kozeschnik, R. Bureau, C. Sommitsch: Computational Materials Science, Vol. 94, 2014, p. 85-94, doi: 10.1016/j.commatsci.2014.02.017

[12] Q. Du, K. Tang, C.D. Marioara, S.J. Andersen, B. Holmedal, R. Holmestad: *Acta Materialia*, Vol. 122, 2017, p. 178-186, doi: 10.1016/j.actamat.2016.09.052
[13] M. Nöhrer, W. Mayer, S. Primig, S. Zamberger, E. Kozeschnik, H. Leitner: *Metallurgical and Materials Transactions A*, Vol. 45, 2014, No. 10, p. 4210-4219, doi: 10.1007/s11661-014-2373-3
[14] M. Nöhrer, W. Mayer, S., Zamberger, E., Kozeschnik, H Leitner: *Steel Research International*, Vol.85, 2014, No.4, p. 679-688, doi: 10.1002/srin.201300185
[15] P. Suwanpinij, H.H. Dickert, N. Thammajak , P. Srichareonchai: *Materials Testing*, Vol. 58, 2016, No.1, p. 5-11, doi: 10.3139/120.110802
[16] K.C. Russell: *Advances in Colloid and Interface Science*, Vol. 13, 1980, No. 3, p. 205-318, doi: 10.1016/0001-8686(80)80003-0
[17] K.G.F. Janssens, D. Raabe, E. Kozeschnik, M.A. Miodownik, B. Nestler: *Computational Materials Engineering - An Introduction to Microstructure Evolution*, 1st ed., Elsevier, Oxford, 2007
[18] E. Kozeschnik, J. Svoboda, F.D. Fischer: *CALPHAD*, Vol. 28, 2004, No. 4, p. 379-382, doi: 10.1016/j.calphad.2004.11.003
[19] E. Kozeschnik, J. Svoboda, F. D. Fischer: *On the choice of chemical composition in multi-component nucleation*, Int. Conference Solid-Solid Phase Transformations in Inorganic Materials, Phoenix, Arizona, J. M. Howe, D. E. Laughlin, J. K. Lee, U. Dahmen, W. A. Soffa, 2005, p. 301-310.
[20] B. Sonderegger, E. Kozeschnik: *Metallurgical and Materials Transactions A*, Vol. 40, 2009, No.3, pp. 499-510, doi: 10.1007/s11661-008-9752-6
[21] Thermodynamic Database 'mc fe.tdb', version 0.014
[22] J. Svoboda, F.D. Fischer, P. Fratzl, E. Kozeschnik: *Materials Science and Engineering: A*, Vol. 385, 2004, No.1, p.166-174, doi: 10.1016/j.msea.2004.06.018
[23] R. Kampmann, R. Wagner: *Decomposition of Alloys: the Early Stages*, 2nd Acta-Scripta Metallurgica Conference, Sonnenberg, Germany, Pergamon, 1983, p. 91-103, doi:10.1016/B978-0-08-031651-2.50018-5
[24] U.F. Kocks: *ASME Journal of Engineering Materials and Technology*, Vol. 98, 1976, No.1, p.76 -85, doi: 10.1115/1.3443340
[25] Y. Bergström: *Review on Powder Metallurgy Physical Ceramic*, Vol. 2, 1983, No. 2, p. 79-265.
[26] L. E. Lindgren, K. Domkin, S. Hansson: *Mechanics of Materials*, Vol. 40, 2008, No. 11, p. 907-919, doi: 10.1016/j.mechmat.2008.05.005
[27] Diffusion Database 'mc fe.ddb', version 1.03
[28] Warczok P., Evaluation of Interfacial Engergies, Technical Paper on MatCalc, 2014.
[29] J. E. Penner-Hahn: X-ray absorption spectroscopy, *Comprehensive Coordination Chemistry II*, J.A. McCleverty, T.J. Meyer, Pergamon, Oxford, 2003, p. 159-186
[30] JJ. Rehr, R.C. Albers: *Reviews of Modern Physics*, Vol. 72, 2000, No. 3, p.621-654, doi: 10.1103/RevModPhys.72.621
[31] W. Klysubun, P. Sombunchoo, W. Deenan, C. Kongmark: *Journal of Synchrotron Radiation*, Vol. 19, 2012, No. 6, p. 930-936, doi: 10.1107/S0909049512040381
[32] M. Nagoshi, T. Aoyama, Y. Tanaka, T. Ishida, S. Kinoshiro ,K. Kobayashi: *ISIJ International*, Vol. 53, 2013, No. 12, p. 2197-2200, doi: 10.2355/isijinternational.53.2197
[33] R. Radis, E. Kozeschnik: *Steel Research International*, Vol. 81, 2010, No. 8, p. 681-685, doi: 10.1002/srin.201000037
[34] R. Lagneborg, T. Siwecki, S. Zajac: *Scandinavian Journal of Metallurgy*, Vol. 28, 1999, No. 5, p.186-241.

[35] T.N. Baker: *Materials Science and Technology*, Vol. 25, 2009, No. 9, p. 1083-1107, doi: 10.1179/174328409X453253
[36] T. Gladman: *The Physical Metallurgy of Microalloyed Steels*, 1st Ed., IOM, London,1997, p. 102.

Acknowledgements
The authors are grateful to the support of MatCalc Engineering GmbH, Dr. Piotr Warczok and the grant TRG5780214 from The Thailand Research Fund (TRF) as well as the Thai - German Seed Fund Project from the Exploratory Research Space @ RWTH Aachen University (ERS).